13th International Symposium on Turbulence and Shear Flow Phenomena (TSFP13)
Montreal, Canada, June 25–28, 2024

THREE-DIMENSIONAL FLOW FIELD AROUND TWO CUBES IN TANDEM

Barbara L. da Silva
Department of Mechanical Engineering
University of Saskatchewan
57 Campus Drive, Saskatoon, Saskatchewan,
S7N 5A9, Canada
barbara.silva@usask.ca

David Sumner
Department of Mechanical Engineering
University of Saskatchewan
57 Campus Drive, Saskatoon, Saskatchewan,
S7N 5A9, Canada
david.sumner@usask.ca

Donald J. Bergstrom
Department of Mechanical Engineering
University of Saskatchewan
57 Campus Drive, Saskatoon, Saskatchewan,
S7N 5A9, Canada
don.bergstrom@usask.ca

ABSTRACT

The mean flow field around two surface-mounted cubes in tandem was investigated through large-eddy simulations at a Reynolds number of $\mathrm{Re} = 1 \times 10^4$ and with a turbulent boundary layer of thickness $\delta/D = 0.8$ at the location of the upstream cube. Center-to-center spacing ratios of $L/D = 2$, 2.5 and 4 were considered to describe the intermittent reattachment, cavity-locked and synchronized shedding regimes, respectively. Although an arch vortex was always present behind the upstream cube, the flow in the gap changed significantly depending on the different flow regimes, with the appearance of a second horseshoe vortex in front of the downstream cube for $L/D = 4$. The mean flow features were related to the near-wall flow field of the downstream cube and the cubes' drag and normal force coefficients. Different near-wall flow field distributions were found depending on whether the flow separated from the upstream cube reattached or impinged on the downstream cube, while the wake of the downstream cube showed base-like vortices for all L/D.

INTRODUCTION

The flow around surface-mounted finite-height square prisms in tandem presents similar regimes to those for two-dimensional or "infinite" square prisms in tandem. These flow regimes change depending on the spacing ratio L/D, where L is the longitudinal center-to-center spacing between the prisms and D is the prisms' width, illustrated in Fig. 1. The regimes for two surface-mounted finite-height square prisms in tandem can be summarized as the single-body or stable reattachment regime ($L/D < 2$), bistable or intermittent reattachment regime ($2 < L/D < 4$), synchronized shedding regime ($4 < L/D < 15$), and an unstable synchronization or quasi-isolated regime ($L/D > 15$) (Sakamoto and Haniu, 1988; Zhao *et al.*, 2021).

Notable differences may be found depending on the prism aspect ratio AR $= H/D$ (where H is the prisms' height). For the case of two surface-mounted cubes (AR = 1) in tandem (Fig. 1), the stable reattachment regime is absent due to some flow always entering the gap between the cubes (Havel *et al.*, 2001). The intermittent reattachment regime was instead found for $L/D < 2.5$, followed by a cavity-locked regime for $2.5 < L/D < 3.3$, in the experiments of Havel *et al.* (2001).

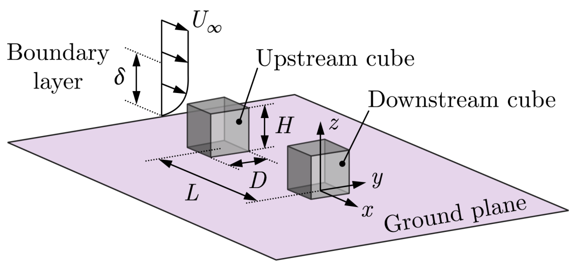

Figure 1. Schematic of two surface-mounted cubes ($H = D$) in tandem.

In the intermittent reattachment regime, two dominant frequencies were found: the lower was related to non-reattaching shear layers separated from the upstream cube, and the higher corresponded to vortex shedding from the downstream cube. In the cavity-locked regime, exclusively described for cubes, the shedding frequency scaled inversely with the spacing between the cubes (Martinuzzi and Havel, 2004). In addition, both the cubes and other surface-mounted finite-height square prisms in tandem feature a gradual increase of the drag force coefficients of the prisms during the intermittent reattachment regime, in contrast to the jump typically found for infinite prisms in tandem (Sakamoto and Haniu, 1988; Havel *et al.*, 2001).

The flow regimes for surface-mounted cubes in tandem have been originally studied based on vortex shedding frequency measurements, flow visualizations, and velocity field measurements at specific locations, with fewer studies (e.g., Paik *et al.*, 2009) considering the three-dimensional flow field. In addition, the connection of the three-dimensional flow field to the near-wall flow and pressure distribution on the downstream cube deserves further attention, since these features are responsible for the aerodynamic forces applied on the cube. The present study aims to revisit the mean flow around two cubes in tandem through large-eddy simulations, which allow for the examination of the mean three-dimensional flow structures in conjunction with the near-wall flow field.

COMPUTATIONAL METHODS

The flow around two cubes in tandem with $L/D = 2$, 2.5 and 4 and $D = 60$ mm was considered to represent the intermittent reattachment, cavity-locked and synchronized shedding regimes, respectively. Large-eddy simulations (LES) were performed with the dynamic Lagrangian subgrid-scale model (Meneveau *et al.*, 1996) and solved with OpenFOAM v7.

The domain size was $25D+L$ in the streamwise (x) direction, $15D$ in the transverse (y) direction and $9D$ in the vertical (z) direction. Blockage effects due to the dimensions in the y and z directions were found to be minimal for the flow around an isolated surface-mounted cube under the same conditions (da Silva *et al.*, 2024), and this behavior is assumed to be the same for the present cubes in tandem. The origin was located at the center of the junction of the downstream cube with the ground plane, as shown in Fig. 1, and the inlet of the domain was fixed at $7.5D$ from the center of the upstream cube.

The domain was discretized with hexahedral grids for all cases. Grid elements are concentrated around the cubes and near the ground plane, giving a total number of elements of 10 379 664, 10 471 596 and 10 599 204 for $L/D = 2$, 2.5 and 4, respectively. The maximum $y_w^+ = y_w u_\tau/\nu$ (where y_w is the wall-normal distance of the closest element and u_τ is the friction velocity) values were 0.7 and 1.4 on the ground plane and cubes' faces, respectively.

No slip boundary conditions were used on the cube and the ground plane, with free slip conditions on the side and top boundaries and a convective outflow condition at the outlet. The inlet had a uniform freestream velocity $U_\infty = 2.5$ m/s prescribed for $z/D > 0.7$ and turbulent boundary layer data mapped for $z/D \leq 0.7$, obtained from a precursor channel flow simulation. These conditions gave a Reynolds number of $\mathrm{Re} = U_\infty D/\nu = 1\times10^4$ (where $\nu = 1.5\times10^{-5}$ m^2/s is the kinematic viscosity) and a turbulent boundary layer with thickness $\delta/D = 0.8$ at the streamwise location of the upstream cube. These conditions were chosen to allow for comparisons with experimental measurements at similar conditions.

Second-order schemes were used for all terms of the conservation equations, except the advective terms of the dynamic Lagrangian model functions, which were discretized with a first order upwind scheme. The flow field was solved with the PISO algorithm and a fixed time step that gave a maximum Courant-Friedrichs-Lewy number of 1.3. After reaching a quasi-steady state, the flow was averaged during 10 s of flow time, equivalent to approximately 30 to 55 shedding cycles depending on the dominant frequency, and the mean flow was averaged over the symmetry of the domain.

To assess the performance of the LES in describing the mean flow field around the cubes in tandem, several mean velocity profiles were compared to particle image velocimetry (PIV) measurements under similar conditions ($\delta/D = 0.8$, $\mathrm{Re} = 7.5\times10^4$) (da Silva, 2023). The mean streamwise velocity component $\overline{u}/U_\infty$ and vertical component $\overline{w}/U_\infty$ along lines located at $y/D = 0$ (the symmetry plane) are presented in Fig. 2, at illustrative streamwise locations of $x/D = -(L/D)/2$ (the middle of the gap) and $x/D = 2$ (the wake of the downstream cube). An overall good agreement was obtained between the simulation results and experimental data for all L/D,

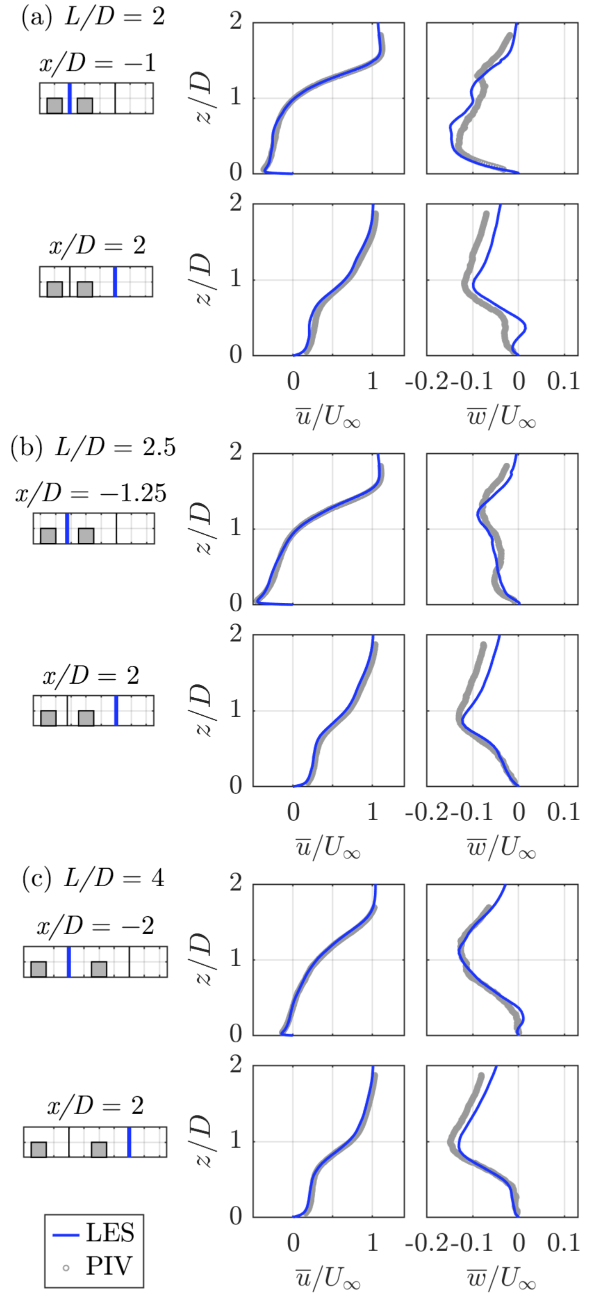

Figure 2. Comparison with experimental results of $\overline{u}/U_\infty$ and $\overline{w}/U_\infty$ profiles at $y/D = 0$ and $x/D = -(L/D)/2$ and 2 for (a) $L/D = 2$, (b) $L/D = 2.5$ and (c) $L/D = 4$.

where the small deviations observed in the $\overline{w}/U_\infty$ profiles are likely due to different parameters in the experiments and simulations, but still within experimental uncertainty. This result suggests that the LES is able to capture the physical features of the mean flow field.

RESULTS AND DISCUSSION

To verify the occurrence of the intermittent reattachment, cavity-locked and synchronized shedding regimes at the chosen spacing ratios, Fig. 3 presents velocity spectra for each L/D condition, as well as for the wake of an isolated cube under the same flow conditions and computational set-up (for more details, see da Silva *et al.* (2024)). The velocity data for the cubes in tandem were sampled at a rate of 5 kHz at a probe

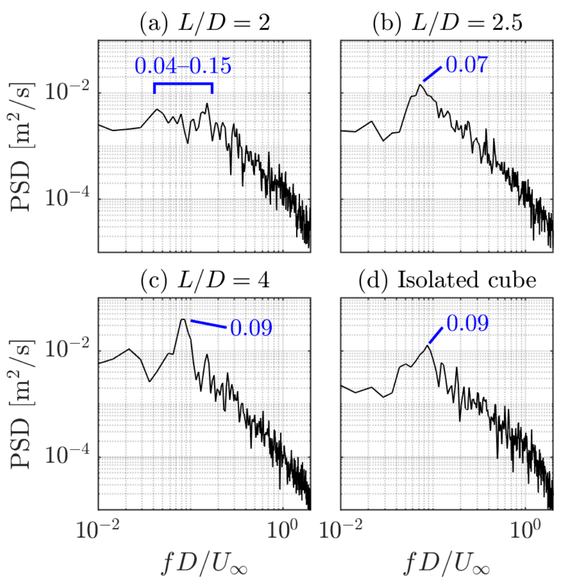

Figure 3. Power spectral density (PSD) in the wake of the downstream cube with (a) $L/D = 2$, (b) $L/D = 2.5$ and (c) $L/D = 4$, and (d) in the wake of the isolated cube.

located at $x/D = 1.5$, $y/D = -0.5$ and $z/D = 0.5$. Similar results were obtained at other locations, although often with more noise due to the quasi-periodic nature of the flow. For the isolated cube, the probe was located further downstream at $x/D = 3$, where the signal was stronger due to the longer formation region of the isolated cube. The spectra were estimated using Welch's method, based on five sets of data with 50% overlap and the Hann window.

The isolated cube (Fig. 3d) shows a Strouhal number $\mathrm{St} = fD/U_\infty = 0.09$ (where f is the frequency). The same dominant frequency is identified for $L/D = 4$ (Fig. 3c), but with a higher-magnitude peak that suggests strengthened vortex shedding. This outcome is consistent with the synchronized shedding regime, where vortex shedding from the downstream cube is enhanced by the periodic impingement of vortices shed from the upstream cube. For $L/D = 2.5$ (Fig. 3b), a single vortex shedding peak was detected, so synchronized shedding also takes place. However, it happens at a lower frequency, which indicates a longer vortex formation region that is consistent with the cavity-locked regime.

For $L/D = 2$ (Fig. 3a), several peaks are found, but two are more prominent at $fD/U_\infty \approx 0.15$ and 0.04. Two frequencies were also detected by Havel *et al.* (2001), who attributed the lower frequency to shedding from the upstream cube, while the higher frequency was due to shedding from the downstream cube. These instances of shedding were hypothesized to occur depending on whether the flow separated from the upstream cube reattached or not on the downstream cube (Havel *et al.*, 2001), characterizing the intermittent reattachment regime.

The vortical structures in the context of the mean three-dimensional flow field around the two cubes in tandem are presented in Fig. 4 for each flow regime and for the isolated cube. Streamlines of the mean velocity field and isosurfaces of $\lambda_2 D^2/U_\infty^2 = -0.5$ and -2 are used to identify these structures, where λ_2 is the second eigenvalue of the tensor $S_{ik}S_{kj} + \Omega_{ik}\Omega_{kj}$, S_{ij} is the strain rate tensor and Ω_{ij} is the vorticity tensor (Jeong and Hussain, 1995). Following the criterion established by Jeong and Hussain (1995), vortices are defined for $\lambda_2 < 0$.

Considering $L/D = 2$ (Fig. 4a), the main structures identified in the flow are the horseshoe vortex of the upstream cube (HSV1), a headband vortex (HBV1) around the upstream cube, which consists of side vortices connected to a free end vortex, and the arch vortices of the upstream (AV1) and downstream (AV2) cubes. The arch vortex AV1 is inclined for this spacing ratio, with its bridge located closer to the upstream cube and its legs extending toward the base of the downstream cube. This shape is an effect of the small gap in which the arch vortex is confined, but the velocity streamlines show that the flow escapes the gap to reattach on the downstream cube both near the feet of the AV1 and near the free end.

The flow field with $L/D = 2$ represents the intermittent reattachment regime, in which the shear layers separated from the upstream cube may either be pushed outward from the gap, causing the low frequency of Fig. 3a, or reattach on the downstream cube's top and side faces, in which case the high frequency prevails (Havel *et al.*, 2001). The outcomes of this regime on the mean pressure coefficient $\overline{C}_p = p/(0.5\rho U_\infty^2)$ (where p is the pressure and ρ is the density) and near-wall velocity field on the downstream cube's faces are shown in Fig. 5a for its front, side and top faces. The front face of the downstream cube presents an overall negative pressure, due to its proximity to the near wake of the upstream cube, but two positive pressure regions are found near the top corners. These regions are characterized by the presence of stagnation nodes $\mathrm{N_F}$, connected by a stagnation saddle point $\mathrm{S_F}$. While this flow distribution may suggest impingement of the flow separated from the upstream cube, the side and top faces contain attachment lines marked by saddle points $\mathrm{S_L}$ and $\mathrm{S_T}$, respectively. The stagnation points on the front face are, therefore, related to type B reattachment (da Silva *et al.*, 2022*a*) of the backward recirculating flow from the top and side, as illustrated in Fig. 6.

For $L/D = 2.5$ (Fig. 4b), the same flow structures as for $L/D = 2$ are observed, but the small increase in L/D has caused the arch vortex AV1 to change significantly. The recirculation region has increased in size, but AV1 has weakened as indicated by the smaller volumes delimited by $\lambda_2 D^2/U_\infty^2 = -0.5$. The larger recirculation region is a feature of the cavity-locked regime, where its extent is controlled by the length of the gap or cavity between the cubes. Its effect on the near-wall flow field of the downstream cube (Fig. 5b) is the occurrence of flow reattachment or impingement very close to the downstream cube's leading edges. The front face shows increased pressure levels and a change in the overall flow pattern, where the focus-saddle-focus bifurcation in Fig. 5a has collapsed to a single node for $L/D = 2.5$.

When L/D is increased to 4 (Fig. 4c), AV1 is stronger and no longer locked to the cavity size, closely resembling that of the isolated cube (Fig. 4d). The flow separated from the upstream cube now impinges on the front face of the downstream cube, leading to the formation of a second horseshoe vortex HSV2. Another consequence is a significant increase of the pressure on the front face of the downstream cube (Fig. 5c), especially surrounding the stagnation points $\mathrm{N_F}$ and $\mathrm{S_F}$.

Vortex cores are observed near the leading edges of the downstream cube for $L/D = 4$, which indicates the occurrence of flow separation and formation of a second headband vortex (HBV2), and is again consistent with the synchronized shedding regime. The pressure field on the side and top faces of the downstream cube (Fig. 5c) shows greater spatial variation, in contrast to the near-zero pressure for $L/D = 2$ and 2.5, and reattachment of the flow separated from the downstream cube's leading edges takes place further downstream. Note that the downstream cube's arch vortex (AV2) does not

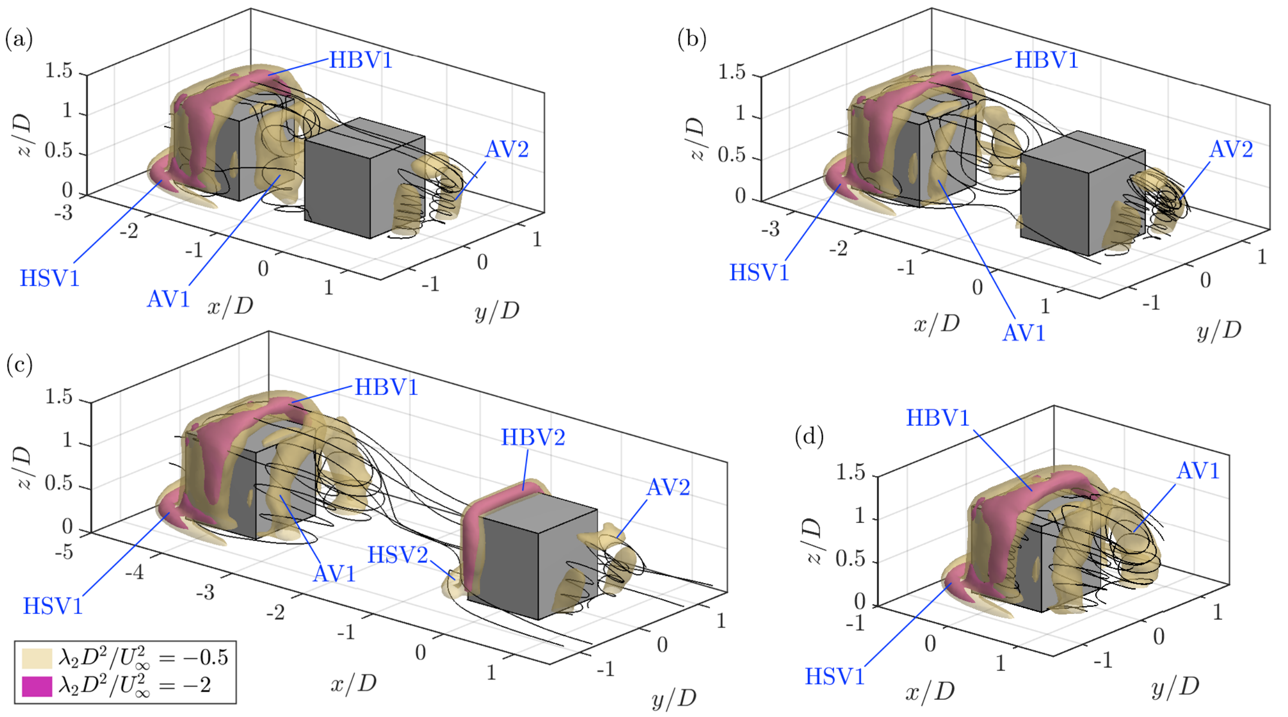

Figure 4. Isosurfaces of the mean $\lambda_2 D^2/U_\infty^2 = -0.5$ and -2 and mean velocity field streamlines in the flow around two cubes in tandem with (a) $L/D = 2$, (b) $L/D = 2.5$, (c) $L/D = 4$ and (d) the isolated cube.

change significantly for the three cases, due to the subsequent separation of the reattached flow from the downstream cube's rear edges for all L/D.

The changes in the near-wall velocity and pressure fields caused by L/D are reflected in the forces exerted on the cubes. Table 1 presents the mean drag force coefficient $\overline{C}_D = \overline{F}_D/(0.5\rho U_\infty^2 D^2)$ and normal force coefficient $\overline{C}_N = \overline{F}_N/(0.5\rho U_\infty^2 D^2)$ of the upstream and downstream cubes, where $\overline{F}_D$ is the mean drag force and $\overline{F}_N$ is the mean normal force.

Marginal changes are observed in the $\overline{C}_D$ of the upstream cube, since the proximity of the downstream cube does not significantly affect the pressure distribution on the front and rear faces of the upstream cube (not shown). A small decrease is found, however, in the value of its $\overline{C}_N$ for $L/D = 2.5$ and 4. A lower $\overline{C}_N$ corresponds to weaker suction, due to a slight increase in the recirculating flow above the upstream cube's free end. For reference, the isolated cube has $\overline{C}_D = 0.97$ and $\overline{C}_N = 0.62$, showing that the proximity of the downstream cube has small effects even for $L/D = 2$.

The downstream cube shows an increasing trend of $\overline{C}_D$ with L/D, which agrees with Havel *et al.* (2001). The drag force is close to zero for $L/D = 2$, as the downstream cube is partially immersed in the upstream cube's wake. On the other hand, the $\overline{C}_N$ of the downstream cube is close to zero for both $L/D = 2$ and 2.5, when the flow mostly skims over the cube's free end as shown in Fig. 5a and b. A significant increase in $\overline{C}_N$ is observed for $L/D = 4$, when the flow separates from the downstream cube.

To consider the wake of the downstream cube in greater detail, Fig. 7 presents the mean velocity field and streamwise vorticity in a y-z plane with $x/D = 2$. Despite the similarity of AV2 between the different cases in Fig. 4a–c, the vorticity distribution changes with L/D, and it is especially different from the one found in the wake of an isolated cube (Fig. 7d). The vorticity of the horseshoe vortex legs, indicated by blue

Table 1. Mean drag force coefficient $\overline{C}_D$ and normal force coefficient $\overline{C}_N$ for the upstream and downstream cubes in tandem.

L/D	Upstream		Downstream	
	$\overline{C}_D$	$\overline{C}_N$	$\overline{C}_D$	$\overline{C}_N$
2	0.93	0.60	−0.01	0.03
2.5	0.92	0.56	0.15	0.05
4	0.93	0.57	0.47	0.22
∞	0.97	0.62	–	–

crosses, is not evident in the wake of the downstream cube. Larger vorticity regions are found instead, corresponding to the diffused vorticity of the upstream (and downstream, for $L/D = 4$) cube's horseshoe vortex and dipole structures. The large streamwise vorticity regions in the upper part of the wake of the isolated cube, which relate to the dipole structures or tip vortices (da Silva *et al.*, 2024), are indicated by a pair of green crosses. This vorticity has disappeared for $L/D = 2$ and only very small regions of the same sign are found for $L/D =$ 2.5 and 4, which may correspond to proto-dipole structures or which may have been induced by other, larger structures of opposite vorticity sign.

These streamwise vorticity regions with opposite sign to the dipole structures are indicated by a red cross in Fig. 7. They have been identified as base-like vortices in Hajimirzaie (2023) and inner vorticity in da Silva *et al.* (2022*b*). The regions change in size and location for the different L/D, showing higher vorticity magnitude and a narrower configuration for $L/D = 2$. This behaviour suggests that, since distinct vortex shedding instances from the upstream and downstream cube

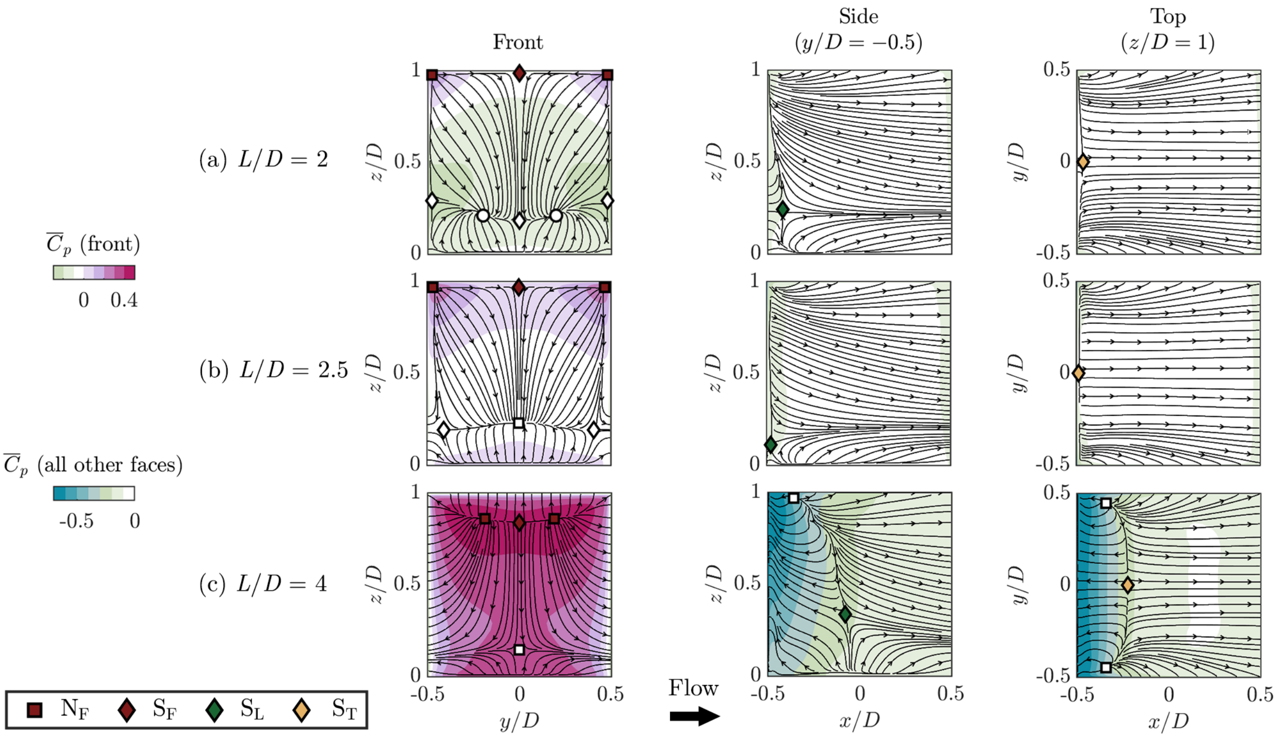

Figure 5. Mean pressure coefficient on the front, side and top faces of the downstream cube and streamlines of the very near-wall velocity field for (a) $L/D = 2$, (b) $L/D = 2.5$ and (c) $L/D = 4$. Some of the node, saddle and focus points are indicated as squares, diamonds and circles, respectively, and notable points are highlighted: the stagnation nodes $\mathrm{N_F}$, stagnation saddle $\mathrm{S_F}$, lateral attachment saddle $\mathrm{S_L}$ and top attachment saddle $\mathrm{S_T}$.

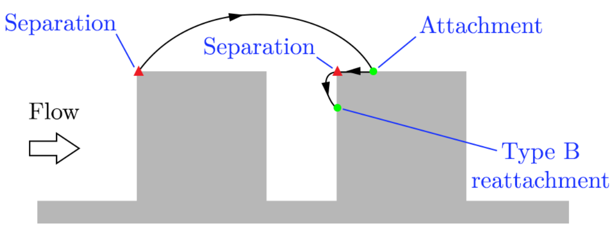

Figure 6. Schematic of type B reattachment on the front face of the downstream cube (not to scale).

are found at this spacing ratio, the base-like vortices could be the time-averaged signature of the vortices shed from the downstream cube, which are more evident for $L/D = 2$. While a different formation mechanism is expected given the fundamental differences from the streamwise vorticity of traditional dipole structures, it is possible that the structures shed from the downstream cube are analogous to the base vortices of surface-mounted finite-height square prisms with quadrupole-type wakes, as inferred by Hajimirzaie (2023). However, further investigation is necessary to verify this hypothesis and the mechanisms involved.

CONCLUSIONS AND FUTURE RESULTS

The major flow structures in the mean flow field around two cubes in tandem with $\mathrm{Re} = 1 \times 10^4$ and $\delta/D = 0.8$ have been identified and related to fluid forces and the near-wall flow field around the downstream cube for spacing ratios $L/D = 2$, 2.5 and 4.

The intermittent reattachment, cavity-locked and synchronized shedding regimes were identified for $L/D = 2$, 2.5 and 4, respectively, based on velocity spectra. For all L/D, the gap region featured mainly the upstream cube's arch vortex, which changed in shape, size and strength depending on the flow regime. However, only small changes were observed in the upstream cube's drag and normal force coefficients, which approached those of the isolated cube.

Flow reattachment on the downstream cube's top and side faces was observed for $L/D = 2$, making its mean drag and normal force coefficients approach zero. The location of reattachment was closer to the leading edges for $L/D = 2.5$, and for $L/D = 4$, the flow impinged on the front face of the downstream cube. This feature caused the formation of a horseshoe vortex and flow separation from the downstream cube's leading edges, accompanied by a significant increase of the drag and normal force coefficients.

While the downstream cube's arch vortex did not change significantly with L/D, it showed a different vorticity distribution to that found in the wake of an isolated cube. "Base-like" or "inner" vortices with signs of rotation opposite to those of traditional dipole structures were found for all L/D. The elucidation of their formation mechanism requires, however, the consideration of the dynamic flow field, to be pursued in future studies.

REFERENCES

Hajimirzaie, Seyed M. 2023, Experimental observations on flow characteristics around a low-aspect-ratio wall-mounted circular and square cylinder, *Fluids* **8**, 32.

Havel, B., Hangan, H. and Martinuzzi, R., 2001, Buffeting for 2D and 3D sharp-edged bluff bodies, *J. Wind Eng. Ind. Aerodyn.* **89**, 1369–1381.

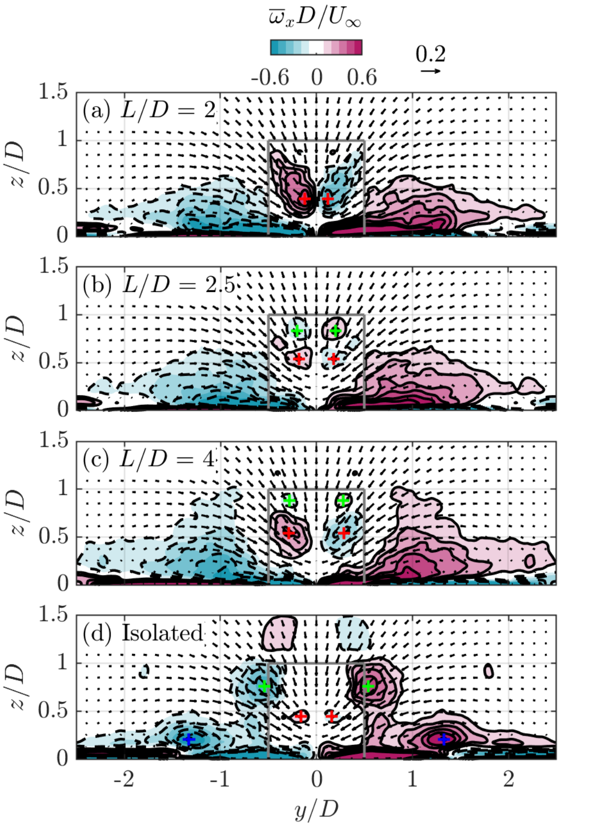

Figure 7. Mean streamwise vorticity distribution and in-plane velocity components in a *y*-*z* plane with $x/D = 2$ for (a) $L/D = 2$, (b) $L/D = 2.5$, (c) $L/D = 4$ and (d) an isolated cube. The red, green and blue crosses indicate the approximate location of the base-like (or inner), dipole (or tip) and horseshoe vortices, respectively.

Jeong, Jinhee and Hussain, Fazle, 1995, On the identification of a vortex, *J. Fluid Mech.* **285**, 69–94.

Martinuzzi, Robert J. and Havel, Brian, 2004, Vortex shedding from two surface-mounted cubes in tandem, *Int. J. Heat Fluid Flow* **25**, 364–372.

Meneveau, Charles, Lund, Thomas S. and Cabot, William H., 1996, A Lagrangian dynamic subgrid-scale model of turbulence, *J. Fluid Mech.* **319**, 353–385.

Paik, Joongcheol, Sotiropoulos, Fotis and Porté-Agel, Fernando, 2009, Detached eddy simulation of flow around two wall-mounted cubes in tandem, *Int. J. Heat Fluid Flow* **30**, 286–305.

Sakamoto, H. and Haniu, H., 1988, Aerodynamic forces acting on two square prisms placed vertically in a turbulent boundary layer, *J. Wind Eng. Ind. Aerodyn.* **31**, 41–66.

da Silva, Barbara L. 2023 Flow around isolated and tandem surface-mounted finite-height square prisms of small aspect ratio. PhD Thesis, University of Saskatchewan, Saskatoon.

da Silva, Barbara L., Hahn, Dylan G. H., Sumner, David and Bergstrom, Donald J., 2022*a*, Mean wake and aerodynamic forces for surface-mounted finite-height square prisms of very small aspect ratio, *Phys. Fluids* **34**, 115118.

da Silva, Barbara L., Sumner, David and Bergstrom, Donald J., 2022*b*, Mean and dynamic aspects of the wakes of a surface-mounted cube and block, *J. Fluids Eng.* **144**, 011302.

da Silva, Barbara L., Sumner, David and Bergstrom, Donald J., 2024, Revisiting the surface-mounted cube: An updated perspective of the near wake and near-wall flow field, *Int. J. Heat Fluid Flow* **106**, 109288.

Zhao, Ming, Mamoon, Abdullah-Al and Wu, Helen, 2021, Numerical study of the flow past two wall-mounted finite-length square cylinders in tandem arrangement, *Phys. Fluids* **33**, 093603.